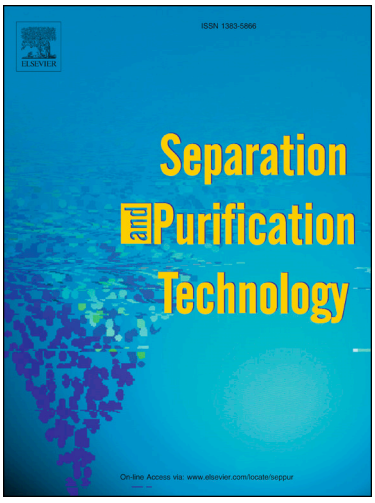

Comparison of microcrystalline and ultrananocrystalline boron doped diamond anodes: Influence on perfluorooctanoic acid electrolysis

Beatriz Gomez-Ruiz, Nazely Diban, Ane Urtiaga

PII: S1383-5866(18)30417-9
DOI: https://doi.org/10.1016/j.seppur.2018.03.044
Reference: SEPPUR 14464

To appear in: *Separation and Purification Technology*

Received Date: 2 February 2018
Revised Date: 20 March 2018
Accepted Date: 21 March 2018

Please cite this article as: B. Gomez-Ruiz, N. Diban, A. Urtiaga, Comparison of microcrystalline and ultrananocrystalline boron doped diamond anodes: Influence on perfluorooctanoic acid electrolysis, *Separation and Purification Technology* (2018), doi: https://doi.org/10.1016/j.seppur.2018.03.044

Comparison of microcrystalline and ultrananocrystalline boron doped diamond anodes: Influence on perfluorooctanoic acid electrolysis

Authors:

Beatriz Gomez-Ruiz, Nazely Diban*, Ane Urtiaga

Department of Chemical and Biomolecular Engineering. University of Cantabria. Av. de Los Castros s/n. 39005 Santander. Spain

* Corresponding Author: dibann@unican.es

Submitted to

Separation and Purification Technology

March 2018

Abstract

This work aims to study the effect of the distinctive chemical and structural surface features of boron doped diamond (BDD) anodes on their electrochemical performance for perfluorooctanoic acid (PFOA) degradation. Commercial BDD anodes were compared: i) a microcrystalline (MCD) coating on silicon; and ii) an ultrananocrystalline (UNCD) coating on niobium. MCD gave rise to the complete PFOA (0.24 $mmol.L^{-1}$) degradation in 4h, at any applied current density in the range 1-5 $mA.cm^{-2}$. On the contrary, only 21% PFOA removal was achieved when using UNCD at 5 $mA.cm^{-2}$ under comparable experimental conditions. Similarly, the total organic carbon (TOC) was reduced by 89% using MCD, whereas only 13% TOC decrease was obtained by UNCD. In order to explain the dissimilar electrochemical activities, the morphological and chemical characterization of the electrode materials was developed by means of FESEM microscopy, XPS and Raman spectroscopy. The UNCD anode surface showed characteristic ultrananocrystalline grain size (2-25 nm), higher boron doping and greater content of H-terminated carbon, whereas the MCD anode was less conductive but contained higher sp^3 carbon on the anode surface. Overall, the MCD electrode features allowed more efficient PFOA electrolysis than the UNCD anode. As a result of their distinctive performance, the energy needed for the maximum PFOA degradation (after 4h) using MCD anode was only 1.4 $kWh.m^{-3}$, while the estimated energy consumption for the UNCD anode would be 37-fold higher. It is concluded that the use of the MCD anode involves considerable energy costs savings.

Keywords

Boron doped diamond (BDD); microscrystalline; ultrananocrystalline; electrolysis; perfluorooctanoic acid (PFOA)

1. INTRODUCTION

In the last two decades, the use of conducting diamond electrodes has grown rapidly due to their extraordinary performance for electrolysis of refractory organic pollutants [1–3]. In pure diamond, each carbon atom is covalently bonded to four other sp^3 hybridized carbons forming an extremely robust and electrical insulator crystalline structure. For most electrochemical applications, some carbon atoms in the lattice are substituted with a dopant to provide electrical conductivity and reduce the wide band gap of diamond. Boron is one of the most interesting doping elements which can act as an electron acceptor and provides diamond with *p*-type semiconductivity at room temperature [1,4,5].

Boron-doped diamond (BDD) film electrodes have gained attention for water treatment by anodic oxidation, due to their unique properties compared to other electrode materials [6–9]. The production and weak adsorption of hydroxyl radicals on the BDD anode result in a low electrochemical activity for the oxygen evolution reaction [3], leading to powerful oxidation conditions for the removal of organic compounds [10–12]. Particularly, BDD electrochemical oxidation has recently demonstrated its efficiency for the abatement of per- and poly-fluoroalkyl substances (PFASs) in aqueous media [13–15]. PFASs, including perfluorooctanoic acid (PFOA) and perfluorooctane sulfonate (PFOS) have been released to the environment because of their use in industrial manufacturing and applications in consumer goods. Persistent PFASs have been detected in industrial effluents, landfill leachates, groundwater, and even in drinking water, causing their bioaccumulation [16,17].

Despite the use of BDD as anode material, the observed rates of PFASs removal were very different among the reported works [13,15,18–24]. Table S1 (in the Supplementary Information) gathers the reported values of the observed kinetic constants alongside the

experimental conditions. Nevertheless, the wide diversity of the experimental conditions, such as area (5.5-140 cm^{-2}), treated volume (0.04-2 L), applied current density (0.15-50 $mA.cm^{-2}$), the initial concentration of PFASs (0.0007-8 mM), and the observed kinetic constants for PFASs degradation hindered the direct comparison of the previous research. Also, it is worth mentioning that the BDD suppliers were different in most of the reported studies, and the relevant characteristics of the BDD coating were not fully detailed, which could explain the diverse electrochemical responses of BDD encountered in the literature.

Many important features of the BDD coatings are known to influence their electrochemical performance as electrodes, including the boron doping concentration, the surface morphology and roughness, the grain size, the content of non-diamond impurities, the surface termination (H or O), and the sp^3/sp^2 carbon ratio of the diamond [5,9,25–28]. The grain size and the surface morphology of BDD electrode depend basically on the operating conditions of the chemical vapor deposition (CVD) synthesis [4,29–32]. CVD leads to the following categories of BDD electrodes: microcrystalline diamond (MCD), nanocrystalline diamond (NCD) and ultrananocrystalline diamond (UNCD). MCD films exhibit grain sizes larger than 1 µm and roughness values that exceed 100 nm [4,33]. However, some applications require much smoother surfaces implying that the grain microsize has to be reduced to the nanoscale. NCD coatings exhibit grain sizes between 10 nm and 1 µm, with low to moderate amounts of sp^2-bonded carbon trapped at defects or grain boundaries. UNCD is the newest material of the diamond coatings family which has attracted significant interest due to its high uniformity, high boundary density and ultra-smooth surface morphology [33–36]. UNCD possesses extremely low grain size (< 10 nm) and roughness (< 100 nm) [4,33].

Though, the small grain size and high grain boundary density of UNCD can facilitate the incorporation of graphitic carbon [35].

In this context, the present work aims to investigate and compare the effect of the surface and crystalline features of two commercial BDD anodes on their electrochemical performance for PFOA electrolysis. The BDD samples used in this study were an UNCD electrode from Advanced Diamond Technologies and a MCD electrode supplied by Adamant Technologies. Great attention has been paid to the effect of the diamond carbon content, boron doping level and the hydrogen contained in the surface, which can play a fundamental role in determining the electrical conductivity and the global electrochemical response of the BDD electrodes.

2. MATERIALS AND METHODS

2.1. Electrode Materials and Chemical Reagents

All chemicals used in the experiments were reagent grade or higher and were used as received without further purification. PFOA ($C_7F_{15}COOH$, 96% purity) was purchased from Sigma Aldrich Chemicals. Ammonium acetate (CH_3COONH_4) and methanol (UHPLC-MS) were obtained from Scharlau. Sodium sulfate (Panreac) 5 $g.L^{-1}$ was used as electrolyte in every electro-oxidation test. All solutions were prepared using ultrapure water (Q-POD Millipore). PFOA aqueous solution with initial concentration 0.24 $mmol.L^{-1}$ were prepared.

The commercial MCD anode was purchased from Adamant Technologies (Neuchatel, Switzerland) as part of a flow-by cell (Diacell 106). The UNCD anode was obtained from Advanced Diamond Technologies (Romeoville, U.S.A.). The MCD anode was formed by a diamond coating of thickness 2–3 μm, synthesized by hot filament CVD on

a monocrystalline p-Silicon circular substrate, with 70 cm^2 of geometrical area. The UNCD anode was made of a boron doped ultrananocrystalline diamond coating of 2 µm film thickness and 3–5 nm average grain size, on a niobium substrate (42 cm^2 of geometrical area). Additionally, three commercial BDD electrodes were purchased from NeoCoat SA (Switzerland) for boron doping calibration (100, 2500 and 10000 ppm of boron, respectively). The latter electrodes were fabricated by hot filament CVD to give a polycrystalline diamond film with 2-3 µm thickness on a p-Silicon substrate, similarly to the MCD anode previously described.

2.2. Electrochemical oxidation of PFOA by BDD electrodes

The electrochemical performance of MCD and UNCD anodes was analyzed by the study of PFOA electrolysis in aqueous solutions. The diagram of the experimental set-up used for the electrooxidation experiments is provided as supplementary information (Figure S1) [14]. Electrolysis tests were carried out in two undivided electrochemical cells, both of them consisting of two parallel electrodes. The feed solution was stored in a feed tank, pumped through the inter-electrode channel at a high linear velocity and recirculated to the feed reservoir. Table 1 collects the details of the experimental conditions applied for each electrochemical cell. The feed volume was adapted to get similar anode area/volume ratios for both experimental systems. The cell was connected to a power supply (Agilent 6654 A) and comparative experiments for MCD and UNCD anodes were conducted under galvanostatic control at j = 5 $mA.cm^{-2}$. Moreover, different current densities were applied for MCD (j = 1 and 2 $mA.cm^{-2}$) and UNCD (j = 10 and 20 $mA.cm^{-2}$) to study the current density effect on the PFOA and total organic carbon (TOC) removal rates. The applied current densities were selected to allow appropriate evaluation of PFOA degradation kinetic during a 4-hour experiment accordingly to the dissimilar electrochemical responses observed for UNCD and MCD

anodes, respectively. Every experiment was conducted in batch mode at constant temperature of 293 ± 2 K. The initial PFOA concentration of the prepared solution was set at 0.24 mmol.L-1 to represent a concentration within the range reported in the literature dealing with PFASs electrochemical oxidation (Table S1, supplementary information). Treated samples were withdrawn from the feed tank at regular time intervals and preserved at 4ºC until analysis. The cell voltages during the electro-oxidation experiments at 5 $mA.cm^{-2}$ were 5.6 and 4.9 V, for MCD and UNCD systems, respectively.

Table 1. Description of the experimental conditions and anode geometry for the electro-oxidation experiments.

Characteristic	**MCD system**	**UNCD system**
Anode geometry	Circular	Rectangular
Anode surface area (cm^2)	70	42
Inter-electrode gap (mm)	5	8
Feed Volume (L)	1	0.5
Flow-rate ($m^3.s^{-1}$)	$5 \cdot 10^{-5}$	$1.1 \cdot 10^{-4}$
Linear Velocity ($m.s^{-1}$)	0.11(1)	0.16
Anode substrate	Silicon	Niobium
Cathode	Stainless steel	Tungsten

(1) Linear velocity was calculated at the central position of the circular electrode

2.3. BDD anodes characterization

The surface morphology of the BBD anodes was determined using field emission scanning electron microscopy (FESEM, JEOL JSM, 7000-F) at 10 kV. The Raman spectra were taken at room temperature under atmospheric pressure in backscattering geometry with a Horiba T64000 triple spectrometer using the 514.5 line of a Coherent Innova Spectrum 70C Ar^+-Kr^+ laser and a nitrogen-cooled CCD (Jobin-Yvon

Symphony) with a confocal microscope and a 100× objective for detection. The power on the sample was kept below 4 mW to avoid laser-heating effects on the probed material and the concomitant softening of the observed Raman peaks. Lorentzian fitting of the Raman spectra was done using Origin 8 software. The relative sp^3/sp^2 band ratios were determined by deconvolution of the spectra obtained from X-ray photoelectron spectroscopy (XPS), using an SPECS (Berlin, Germany) system equipped with a Phoibos 150 1D-DLD analyser and monochromatic Al K_α radiation (1486.6 eV). Data analysis was carried out using Casa XPS 2.3.16 Software to fit the signals to Gauss-Lorentzian curves, after removing the background (Shirley).

2.4. Analytical procedures

PFOA concentration in the MCD experiments, was determined by HPLC-TQD mass spectrometry (Acquity, Waters), and the X-Bridge BEH C18 (2.5 µm, 2.1 x 75 mm) column. The eluents were: (i) an aqueous solution containing ammonium acetate (CH_3COONH_4) 2 $mmol.L^{-1}$ and 5% of methanol, and (ii) pure methanol. The eluent flow rate was 0.15 $mL.min^{-1}$. The limit of quantification (LOQ) was 1 $\mu g.L^{-1}$. For experiments using the UNCD anode, the PFOA content was analyzed using HPLC-DAD (Water 2695) equipped with a X Bridge C18 column (5 µm, 250 mm x 4.6 mm, Waters). A mixture of methanol (65%) and di-hydrogen phosphate (35%) was used as mobile phase in isocratic mode with a flow rate of 0.5 $mL.min^{-1}$. The wavelength of the detector was set at 204 nm. The LOQ was 7.4 $mg.L^{-1}$ [37]. Total organic carbon (TOC) analyses were performed using a TOC-V CPH (Shimadzu). Fluoride was analyzed by ion chromatography (Dionex 120 IC) provided with an IonPac As-HC column and using a 9 $mmol.L^{-1}$ Na_2CO_3 solution as eluent, that was circulated at a flowrate of 1 $mL.min^{-1}$, based on Standard Methods 4110B [38]. The LOQ for fluoride analysis was 0.03 $mg.L^{-1}$.

3. RESULTS AND DISCUSSION

3.1. PFOA electrolysis

Figure 1 reports the effect of the applied current density on the PFOA removal rate using MCD (Figure 1a) and UNCD (Figure 1b) anodes. Different electrochemical responses were observed for both materials. MCD anode allowed a sharp abatement of PFOA, which was almost completely degraded in only 4 hours, independently of the applied current density.

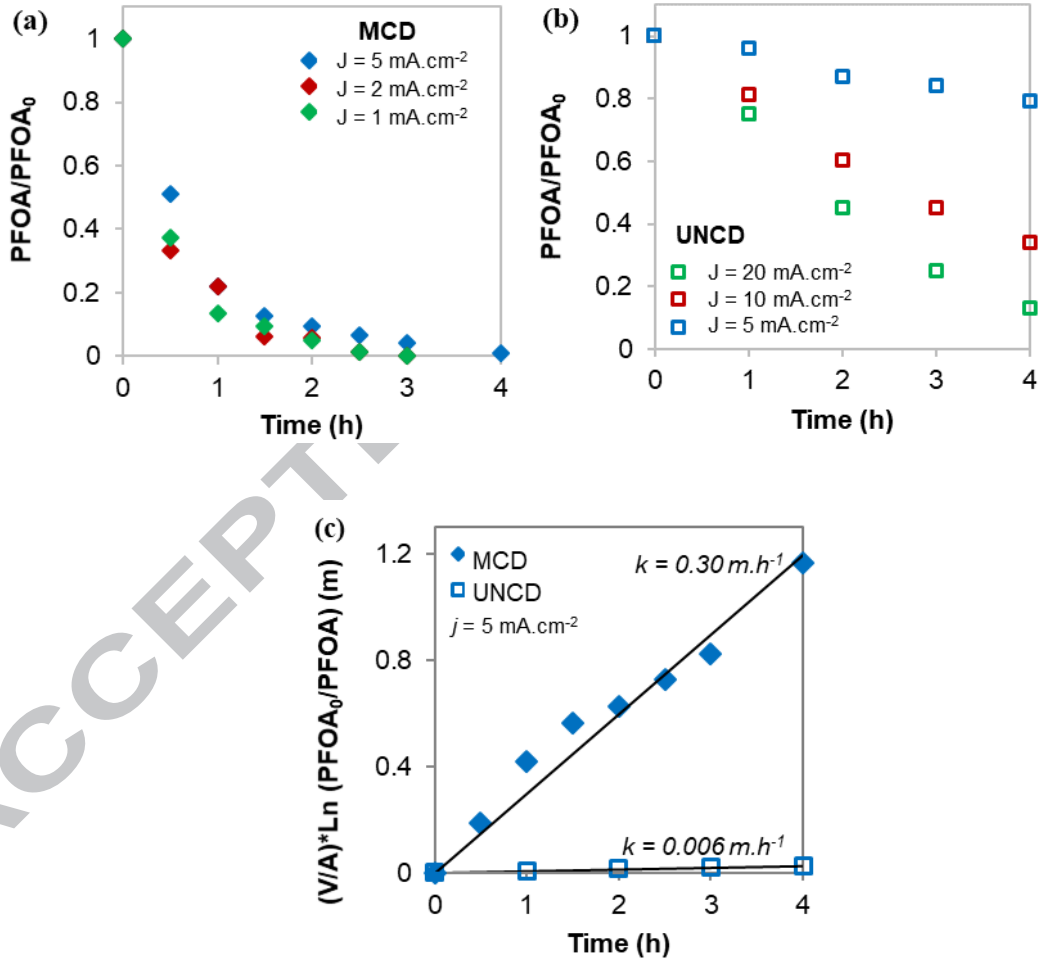

Figure 1 (1.5-column fitting image). Influence of the applied current density on PFOA removal with the treatment time, using: (a) MCD (j = 1, 2 and 5 mA.cm^{-2}) and (b) UNCD (j = 5, 10 and 20 mA.cm^{-2}). (c) Fitting of the experimental data obtained at j = 5 mA.cm^{-2} to the kinetic model (Eq. 2) for both electrodes. The experimental standard

deviation of MCD anode (a) was in the range of 10-15% and therefore experimental curves at j = 1–5 mA.cm^{-2} had no significant difference. In the case of UNCD (b), the standard deviation of 3-7% demonstrated that the effect of the current density under the range 5-20 mA.cm^{-2} on PFOA electro-oxidation was statistically significant. $[PFOA]_0$ = 0.24 mmol.L^{-1}

Therefore, for the MCD anode, increasing j in the range 1 - 5 mA.cm^{-2} had the effect of increasing the energy consumption of the process. On the contrary, the UNCD anode provided significantly slower PFOA degradation kinetics. When using UNCD, 21, 66 and 87 % PFOA removals were achieved at j = 5, 10 and 20 mA.cm^{-2}, respectively. It is worth mentioning that the enhancement of PFOA degradation by sodium sulfate electrolyte as a promoter of secondary oxidant species was considered to be negligible at the low range of current densities applied in the present study [37,39]. Consequently, the remarkable lower PFOA removal ratios alongside the substantial effect of the applied current density observed for the UNCD film resulted in its less efficient electrochemical performance compared to the MCD anode.

The comparison of experimental systems for MCD and UNCD anodes was performed by means of the apparent kinetic rate. The PFOA mass balance in the electrochemical system is written as follows:

$$V \frac{\partial C}{\partial t} = -k\, A\, C \qquad \text{(Eq.1)}$$

where V is the volume of the treated solution (L), C is the PFOA concentration (mmol.L^{-1}) in the feed tank, t is the electro-oxidation time (h), k is the apparent first order kinetic constant of PFOA degradation (m.h^{-1}) and A is the electrode surface area (m^2). The integration of Eq. (1) during the length of the experiment (t) results in Eq. 2.

$$(V/A)\,Ln\left(\frac{C_0}{C}\right) = -k\,t \qquad \text{(Eq.2)}$$

PFOA removal data using MCD and UNCD electrodes, at the same applied current density j= 5 mA.cm^{-2}, were fitted to Eq. (2) in Figure 1c. The definition of k allows to remove the effect of the anode area and treated volume for comparison. Table 2 collects the values of k for MCD and UNCD anodes at the different applied current densities that were tested. In the MCD system, the PFOA decays were fitted to first-order kinetics, and the values of the kinetic constants remained very similar when increasing the applied current densities. This behavior has been previously described in the literature; the degradation of the perfluoroalkyl pollutant occurred through a fast series of reactions in which both direct electron transfer and oxidation by electro-generated hydroxyl radicals took place, and the overall kinetics were controlled by the mass transport of PFOA from the liquid bulk to the anode surface [40,41]. On the other hand, the PFOA decomposition trend obtained by means of UNCD anode at j = 5 mA.cm^{-2} could be described by either zeroth-order or first-order kinetics. Moreover, the values of the kinetic constant were much lower compared to the ones obtained in the MCD system, and they gradually raised when increasing j. This electrochemical performance pointed out the limited availability of active sites on the surface of UNCD anode for direct electron transfer and hydroxyl radical production, which play the main roles in PFOA electrochemical degradation [23,24].

The kinetic constants obtained in the present study for the UNCD anode are in agreement with the data reported by Schaefer et al. [15] for PFOA electrolysis using an UNCD electrode manufactured by the same provider (Table 2). Furthermore, Soriano et al. [22] studied the electrochemical removal of perfluorohexanoic acid (PFHxA), which contains two fluorinated carbons less than PFOA in the perfluoroalkyl chain, using an

electrochemical cell that contained two parallel flow-by compartments made of a central bipolar BDD/Si electrode and two BDD/Si anode and cathode. In the latter case [22], the provider of the BDD electrodes was the same as the manufacturer of the MCD anode used in the present study. The reported kinetic constant for PFHxA (870 $mg.L^{-1}$) removal was 0.13 $m.h^{-1}$ at j = 5 $mA.cm^{-2}$, that is moderately slower than the PFOA degradation constant using the MCD anode in the present work (0.30 $m.h^{-1}$), although k values were still within the same order of magnitude. The comparison of the kinetic constants of both MCD and UNCD anodes together with the results reported in the literature indicates that the PFOA degradation rates provided by UNCD/Nb electrodes were much slower than in case of using MCD/Si.

Table 2. Apparent kinetic constants k ($m.h^{-1}$) for the PFOA electro-oxidation on BDD anodes and the comparison with previous studies using similar electrodes. Reference [22] studied the degradation of PFHxA instead of PFOA.

MCD/Si (this study)		**UNCD/Nb (this study)**		**UNCD/Nb** [15]		**MCD/Si (bipolar)** [22]	
j ($mA.cm^{-2}$)	k ($m.h^{-1}$)	j ($mA.cm^{-2}$)	k ($m.h^{-1}$)	j ($mA.cm^{-2}$)	k ($m.h^{-1}$)	j ($mA.cm^{-2}$)	k ($m.h^{-1}$)
1	0.31	5	0.006	3	0.0054	5	0.126
2	0.36	10	0.027	15	0.026		
5	0.30	20	0.048	50	0.086		

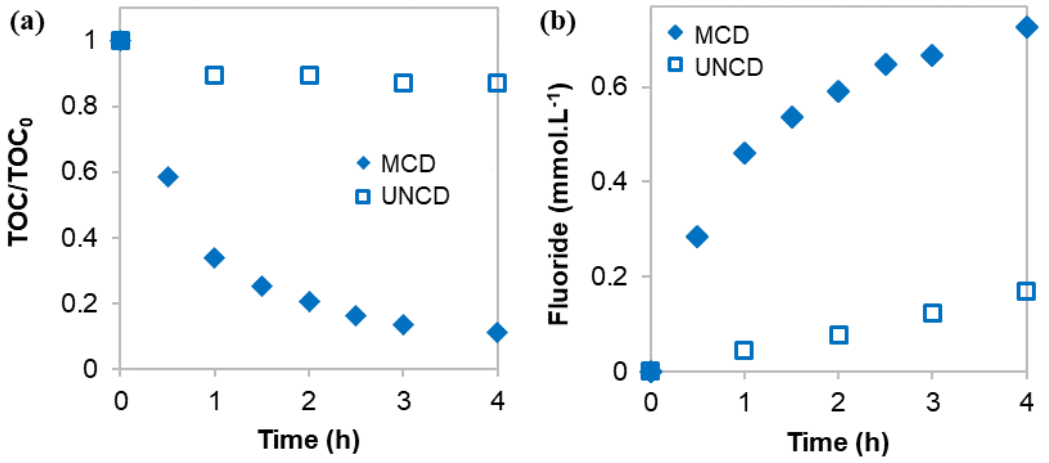

Figure 2 (1.5-column fitting image). Evolution of: (a) TOC/TOC_0 and (b) fluoride concentration with the electrolysis time, using MCD and UNCD anodes at j = 5 mA.cm^{-2}. $[PFOA]_0$ = 0.24 mmol.L^{-1}

In addition, PFOA mineralization was confirmed by the progress of TOC disappearance and the fluoride release using MCD and UNCD anodes (Figure 2a). Similarly to PFOA removal trends, the reduction of TOC was influenced by the type of anode. At j = 5 mA.cm^{-2} and t = 4 h, TOC was reduced by 89% using MCD, whereas only 13% TOC decrease was obtained using the UNCD anode. The effective cleavage of C-F bonds was verified by the release of fluoride in the solution (Figure 2b). The final F^- concentration was 0.7 and 0.3 mmol.L^{-1} for MCD and UNCD systems, respectively, after 4h of the treatment at j = 5 mA.cm^{-2}. These results are in agreement with the higher PFOA decomposition rate on the MCD electrode.

Moreover, previous research [20,42] discussed the role of the fluoride released upon PFOA degradation on the anode surface fluorination. This mechanism could improve PFOA degradation, as reported for F-doped Ti/SnO_2 electrodes [43]. Thus, in order to investigate the influence of fluoride, additional tests were carried out with the MCD anode at j = 5 mA.cm^{-2}, by adding sodium fluoride to the feed solution. Similar first-

order PFOA removal rates (0.27 and 0.26 $m.h^{-1}$, respectively) were observed when adding 20 and 50 $mg.L^{-1}$ of fluoride, that were similar to the degradation kinetics obtained without any extra fluoride addition. In the same way, TOC depletion was not accelerated by the addition of the different contents of F^- into the reacting media. Moreover, to contrast if higher current densities than those used in the present system could promote the fluorine formation, a test was done at 20 $mA.cm^{-2}$. The kinetics observed in Figure S2 (Supplementary information) for TOC removal, did not reflect any improvement to those experiments done at lower *j*. Therefore, the PFOA electrochemical oxidation by means of MCD anodes was not enhanced by the fluoride released into the solution during the degradation process.

3.2. Characterization of the BDD electrodes and its influence on PFOA electrolysis

According to the literature [5,26,44], the anodic reactions on BDD electrodes could be influenced by (i) boron doping level, (ii) morphological features and (iii) diamond carbon content, as it has been described for other organic compounds. Therefore, due to the different electrochemical response of the two commercial BDD anodes that have been found in this study as well as the diverse results of PFAS removal rates reported in the literature (Table S1), the surface chemical and morphological characterization of MCD and UNCD anodes was studied to elucidate its effect on PFOA electrolysis.

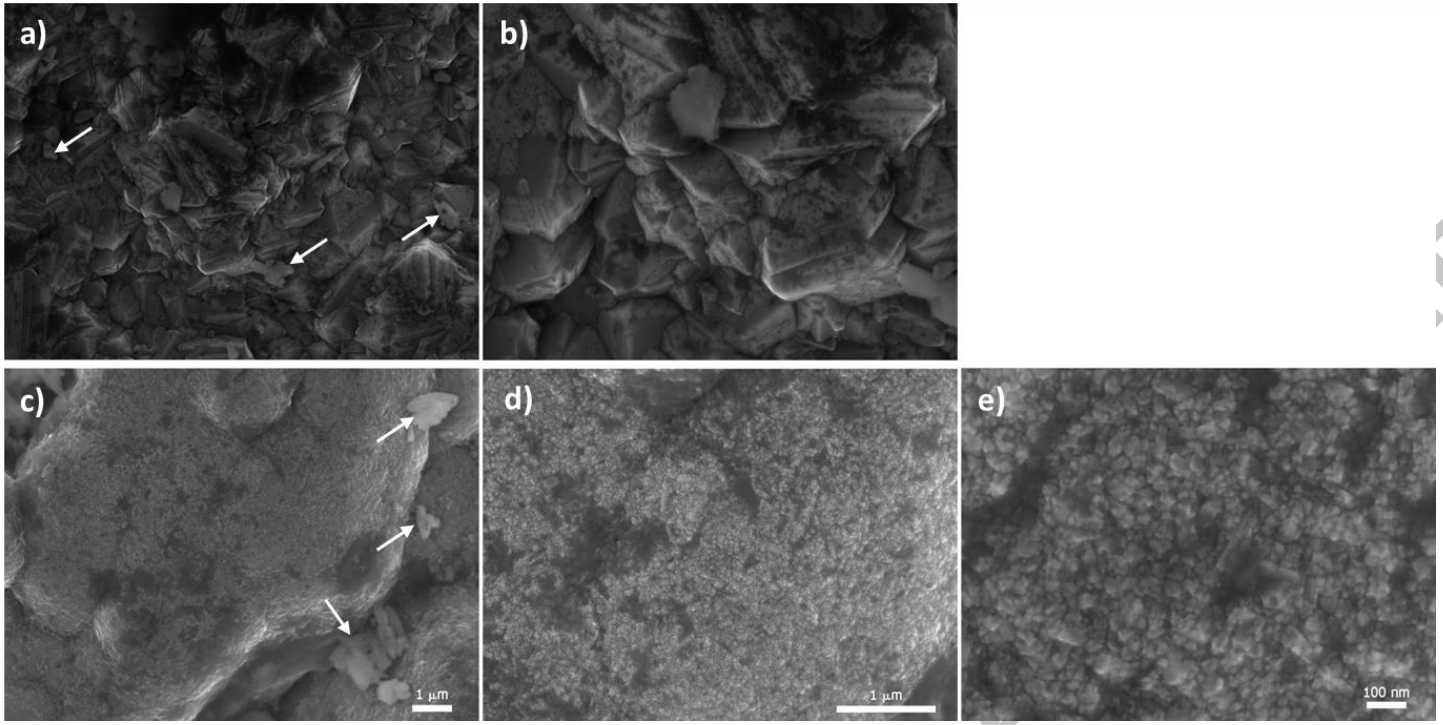

Figure 3 (2-column fitting image). FESEM surface images of MCD at ×10000 (a) and ×25000 magnification (b), and UNCD at ×10000 (c), ×25000 (d) and ×100000 magnification (e). Scale bars indicated for each magnification. Arrows indicate dirtiness of salt deposits on the anode surface after the experiments.

Figure 3 shows FESEM surface images of the MCD and UNCD anodes. The FESEM images confirm the information provided by the manufacturers. At ×10000 and ×25000 magnifications MCD shows the expected microcrystalline structure with crystal grains in the range of approximately 1-3 μm while at the same magnifications, the crystals cannot be appreciated in the UNCD anode. Nevertheless, at ×100000 magnification nanocrystal grains ranging approximately between 2-25 nm could be observed in UNCD surface [45]. The surface images present well faceted microcrystalline diamond for MCD and line-granular ultrananocrystalline diamond for UNCD film [35]. Moreover, it is worth mentioning that the diamond grains were homogeneously distributed over the anode surface and no cracking defects were appreciated.

Figure 4 presents Raman spectra obtained for MCD (Figure 4a) and UNCD (Figure 4b) anodes [35,46]. The values of the peaks were determined by deconvolution of Raman spectra using Lorentzian functions (green lines). MCD Raman spectra showed a sharp characteristic peak of microcrystals of diamond facet {111} at 1329 cm^{-1} slightly shifted from the typical 1333 cm^{-1}, characteristic of pure diamond microcrystals. Indeed, its actual position depends on the boron concentration in the diamond lattice, and moves to lower wavenumbers with increasing boron concentration, as reported by [47,48]. The characteristic peaks at 1350 and 1550 cm^{-1} of D (sp^2 carbon impurities) and G (non-diamond sp^2- bonded carbon atoms in the grain boundaries, C-H bending bonds) bands respectively could be also observed (peaks at 1387 and 1547 cm^{-1} in Figure 4a).

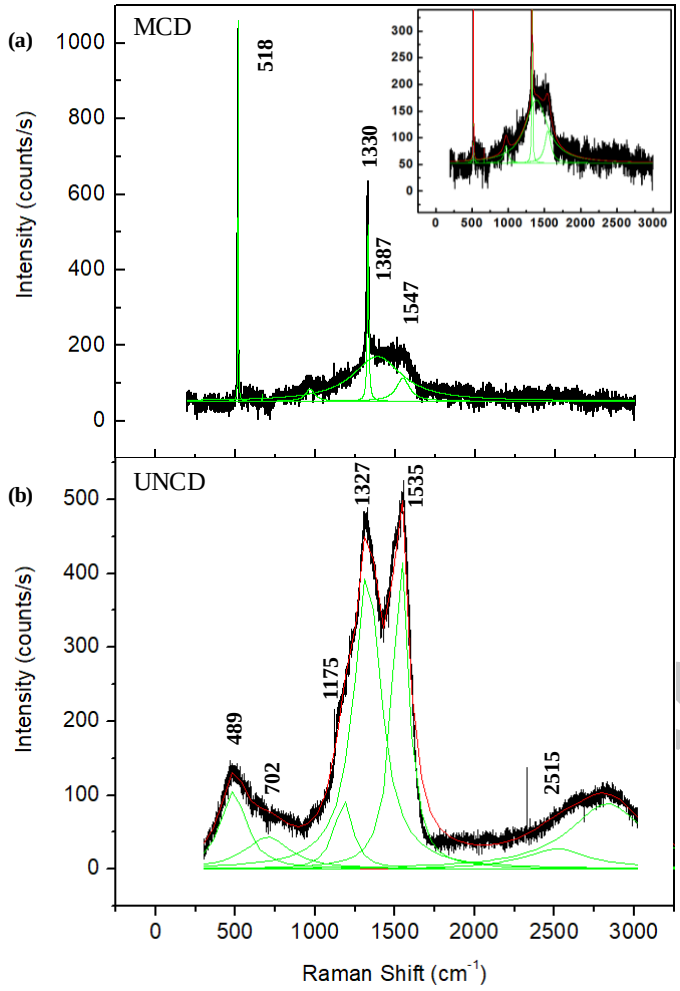

Figure 4 (single column fitting image). Raman spectra of (a) MCD and (b) UNCD electrodes. The values of the peaks were determined by deconvolution of Raman spectra using Lorentzian functions within the software Origin 8 (green lines).

On the contrary, UNCD surface (Figure 4b) presents a wide peak at 1327 cm^{-1} combining the sp^3 diamond at 1333 cm^{-1} and a more dominant D band (1310–1450 cm^{-1}) coming from the presence of disordered carbon at the grain boundary [35,49]. Besides G band characteristic of sp^2 carbon at 1535 cm^{-1}, as well as the G' band at 2515 cm^{-1} could be identified in UNCD anode. The peak at 1175 cm^{-1} which was formerly [49] ascribed wrongly to transpolyacetylene (typically at 1150 cm^{-1}), has been demonstrated to actually correspond to CH_x bonds in the grain boundaries of nanocrystralline

diamonds [50]. The UNCD spectrum in Figure 4b is a typical Raman spectrum of ultrananocrystalline diamonds using a laser excitation at 514 nm. According to the literature [4], the small diamond grain size in the UNCD electrode produced a large presence of graphite in the boundary layers that scattered phonons to make the D peak intensity at 1357 cm^{-1} being ~ 57 times larger than the diamond peak at 1333 cm^{-1}.

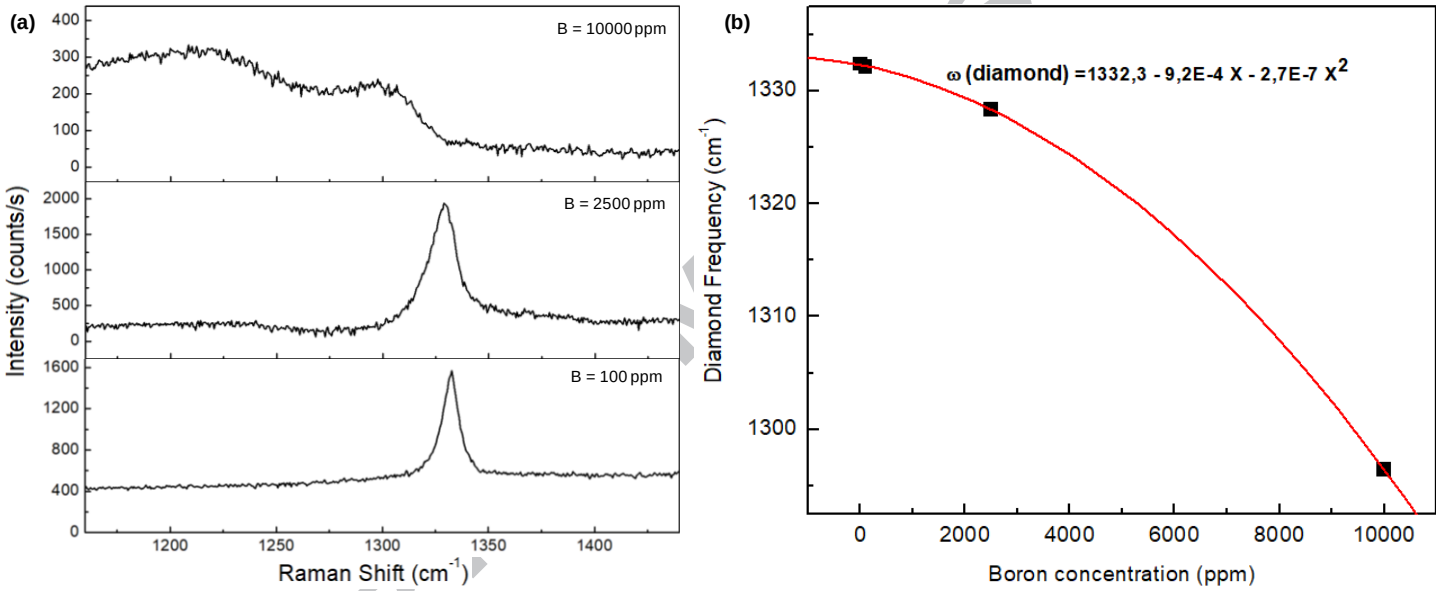

Figure 5 (2-column fitting image). (a) Raman spectra of microcrystalline BDD standards with different boron concentration: 10000 ppm, 2500 ppm and 100 ppm. (b) Diamond frequency (cm^{-1}) as a function of the boron concentration (ppm) in BDD standards obtained from Raman spectroscopy.

The displacement of the diamond peak to lower frequencies in microcrystalline BDD materials is proportional to the increase of boron content, according to May et al. [46]. This property has been applied in the present work to determine the concentration of boron in the diamond lattice of the MCD electrode. A calibration curve was built using 3 commercial microcrystalline BBD electrodes (NeoCoat, Switzerland) as standards

with known boron concentrations of 100, 2500 and 10000 ppm, respectively. Figure 5a shows the Raman spectra for each BDD standard and the displacement of the Raman shift of the diamond peak for each standard was determined. The pure diamond peak frequency was used as reference (0 boron concentration, 1333 cm^{-1}). The calibration curve that relates the boron concentration with the diamond Raman vibration frequency in cm^{-1} is represented in Figure 5b. From this calibration curve, the boron concentration for the MCD electrode was calculated as 1676 ppm. Similarly for boron doped ultrananocrystalline diamonds, it has been reported [35] that the D band peak shifted from 1355 cm^{-1} at B/C ratios of 0 ppm towards 1300 cm^{-1} at B/C ratios of 6000 ppm. A comparison between the Raman spectrum of the UNCD anode and the Raman spectra of ultrananocrystalline BDDs at different boron doping levels reported by Zeng et al. [35] indicated that our UNCD anode would have a boron content of approximately 3000 ppm.

For further surface characterization, Figure 6 depicts the XPS C 1s spectra of the MCD and UNCD anodes. The peak at 284.5±0.1 eV was labelled as $C–C_1$ and the component $C–C_2$ was shifted +0.9 eV. These peaks were attributed to hydrogenated and non-hydrogenated carbon diamond, respectively [51,52]. The peak at 283.4±0.3 eV was ascribed to C=C sp^2 carbon or graphitic defects at the diamond surface and oxygenated carbon species were detected at higher binding energies: 286.5, 287.5 and 289.3 eV for single oxidized components (C–O) such as i.e. –C–OH and –C–O–C– bonds, and further oxidized groups as –C=O or –COOH [51]. The oxidized carbon species typically appear after usage as a result of anode ageing. The B-C peak of boron doped diamonds that should appear at approximately 282.6 eV is not usually observed in these materials due to the presence of surface defects that affect the surface Fermi level [52]. It can be seen that the major component of the MCD surface is $C–C_2$ or sp^3 crystal diamond

carbon (56.0%), the contribution of $C–C_1$ or hydrogenated diamond was 16.1%, the total oxygenated species were 23.3% and graphitic defects counted up to 4.6% of the total carbon of the MCD anode. On the other hand, the major component of UNCD anode is hydrogenated diamond carbon ($C–C_1$) with 35.2%, non-hydrogenated diamond ($C–C_2$) accounted for 31.1%, the graphitic carbon was 5.4% and oxidized species were 28.3% of the total carbon. Hydrogen-terminated diamond ($C–C_1$) is produced during the BDD synthesis under H_2-rich conditions to avoid the formation of graphitic carbon at grain boundaries [4]. The higher content of ($C–C_1$) of the UNCD is related to the smaller (ultranano) grain size and consequently higher grain boundary density [52]. The amount of oxygenated species on both diamond films was comparable (23.3 vs 28.3% for the MCD and UNCD anodes, respectively), which is related to the formation of hydroxyl radicals during the uses of the materials for anodic oxidation [9].

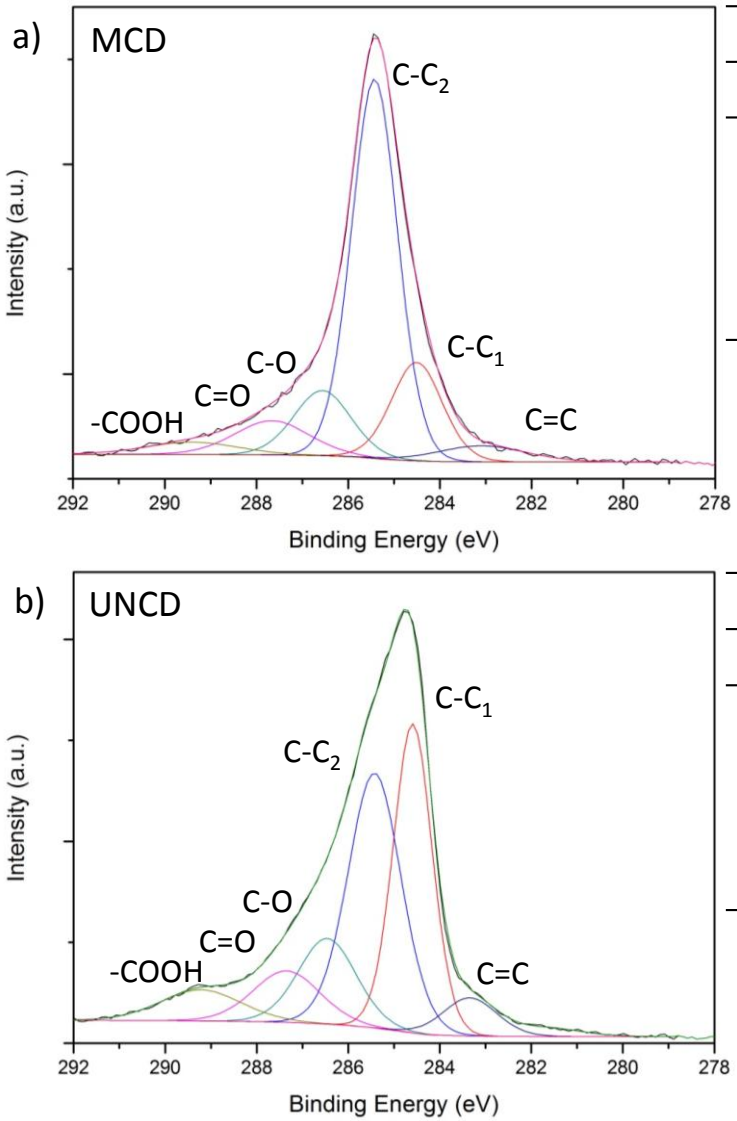

MCD	
Component	**Amount (%)**
C-C_1 (C-H)	16.1
C-C_2 (sp^3)	56
C=C (sp^2)	4.6
C-O	23.3

UNCD	
Component	**Amount (%)**
C-C_1 (C-H)	35.2
C-C_2 (sp^3)	31.1
C=C (sp^2)	5.4
C-O	28.3

Figure 6 (1.5-column fitting image). XPS C1s spectra of (a) MDC and (b) UNCD electrodes. -COOH, C=O and C-O were assigned to oxygenated carbon species. C-C_1 and C-C_2 corresponded to hydrogenated and non-hydrogenated carbon diamond, respectively, and C=C sp^2 refers to the graphitic defects in the diamond surface. Peaks were fitted to the spectra using Gauss-Lorentzian functions.

Overall the following remarkable differences about BDD films characterization can be highlighted: i) the sp^3 diamond relative carbon abundance on the MCD surface is 1.8 times higher than on UNCD surface, ii) lower boron doping level was found in MCD

material compared to UNCD anode, and iii) the hydrogen-terminated diamond on MCD is 2.2 times lower than in UNCD.

Thus, some studies have demonstrated that higher content of sp^3 carbon resulted in more rapid and efficient contaminant decay by electrochemical oxidation [5,25,26]. Assuming that the sp^3 diamond is the direct responsible of the formation of hydroxyl radicals on the anode surface for electrooxidation applications, a lower abundance on sp^3 diamond carbon would might imply lower hydroxyl radical generation per unit anode surface area [25,26]. The sp^2 or graphitic carbon content is very similar in both anodes (MCD = 4.6% and UNCD = 5.4%) and thus, the lower PFOA degradation efficiency of UNCD anode encountered in the present work cannot be justified by differences in the grain boundary graphitic defects. The introduction of boron atoms into the diamond lattice is the main mechanism responsible for the conductivity and the density of active sites on the surface [53]. The anodic materials herein compared present a boron doping level of 1600 (MCD) and 3000 ppm (UNCD). However, despite the higher boron doping level of UNCD anode, the PFOA degradation efficiency was not improved, possibly related to the distortions or defects added into the lattice hindering the electrochemical activity [54,55]. The presence of H-terminated carbon also favors the p-type electrical conductivity on the conductive diamond film surface and enhance the surface hydrophobicity, electron affinity and conductivity [56]. However, the superficial hydrogen content can be progressively changed to O-terminated surface during the electro-oxidation treatments, which would cause the anode surface oxidation and its consequent passivation.

According to the XPS and Raman analysis, UNCD possessed higher boron doping and more H-terminated superficial carbon content than MCD material, a sum of

characteristics that could improve the UNCD *p*-type superficial conductivity [53,57]. This assumption was verified by the cyclic voltammetry (CV) of PFOA solution using sodium sulfate electrolyte, of both BDD anodes. Figure S3 given in the Supplementary Data shows that higher current densities were recorded for the UNCD electrode (Figure S3b), because of its more elevated electrical conductivity. Moreover, a distinctive feature is observed for the MCD anode, as its cyclic voltammogram (Figure S3a) shows the PFOA direct oxidation peak at a potential close to 2.6 V, which is neither observed in the CV with the single Na_2SO_4 electrolyte solution, nor in the case of UNCD anode (Figure S3b).

Overall, the higher sp^3 carbon content, lower hydrogen terminated carbon and lower conductivity of the MCD film seem to favour the faster and more efficient PFOA degradation. On the contrary, the surface features, such as extremely small grain size, lower sp^3 carbon abundance and higher conductivity, of the UNCD electrode provided a limited electrochemical activity for the PFOA removal.

Finally, the practical feasibility of the electrochemical technology is often linked to the energy consumption. The energy consumption (W, $kWh.m^{-3}$) is directly related to the specific electrical charge (Q, $kAh.m^{-3}$) and the cell potential (v), as described in equation 3 [58]:

$$W = Q \cdot v = \frac{j\,A\,t}{V} \cdot v \qquad \text{(Eq.3)}$$

Due to the different electrochemical behavior exhibited by the MCD and UNCD anodes, the energy consumption has been calculated for the maximum PFOA degradation rate obtained in each system, which was 99% and 87% after 4h of treatment, respectively. In this way, the energy consumption estimated for PFOA

removal using MCD was only 1.4 kWh.m^{-3} (j = 1 mA.cm^{-2}). On the contrary, using UNCD anode would imply shifting to a higher current density (j = 20 mA.cm^{-2}) that implies an estimated consumption of 52.4 kWh.m^{-3}. These results confirmed that the differences on BDD surface features can influence on the reaction time and the current density needed for the contaminant removal which impacts directly on the energy costs of the electrochemical process.

Additionally, to determine the efficiency of the electro-oxidation process, the decrease in pollutant concentration during electrolysis can be represented against specific electrical charge (Q). To illustrate this point, the variation of PFOA degradation rate with Q was plotted in Figure S4 in the Supplementary material. It can be seen that for the MCD system, the increase in current density from 2 mA.cm^{-2} to 5 mA.cm^{-2} significantly decreased the oxidation efficiency. Therefore, current densities higher than 5 mA.cm^{-2} only lead to a massive loss of current efficiency in this process. During PFOA electrolysis by UNCD anode (Figure S4b), the concentration decreased with the increase of specific electrical charge with similar trends for all the applied current densities from 5 to 20 mA.cm^{-2}. In conclusion, to achieve satisfactory PFOA removal rates, e.g.: 90% removal, the specific electrical charge passed was two orders of magnitude larger for UNCD anode than MCD electrode.

4. CONCLUSIONS

This work reports a morphological, chemical and electrochemical comparison of two BDD electrodes that are commercialized for anodic oxidation. Attending to their crystal size the electrodes are classified as microcrystalline diamond (MCD) and ultrananocrystalline diamond (UNCD). The relationship of the anode surface features

with their performance in the electrolysis of perfluorooctanoic acid (PFOA) was analyzed. The following considerations can be withdrawn from the reported results:

- Electrochemical oxidation of PFOA by means of the MCD anode was significantly more efficient than when using the UNCD electrode. The MCD anode led to the complete degradation of the persistent pollutant in 4 h, at any applied current density in the range of 1-5 $mA.cm^{-2}$. Conversely, remarkable lower PFOA removal ratios were achieved by the UNCD anode, as only 21% PFOA removal was achieved in 4 h working at 5 $mA.cm^{-2}$.
- FESEM microscopy confirmed the micro and ultrananocrystalline structure for MCD and UNCD anodes, respectively. Moreover, the higher sp^3 carbon content and lower boron content and H-terminated carbon content of the MCD, revealed by Raman and XPS spectroscopy, seem to favor faster and more efficient PFOA degradation. On the contrary, the ultrananocrystalline surface features and the higher conductivity of UNCD anode limited the electrochemical activity for PFOA electrolysis.
- Different electrochemical behaviors of the MCD and UNCD BDD anodes strongly impacted the process energy consumption. The energy needed for PFOA removal from a 0.24 $mmol.L^{-1}$ solution was 1.4 $kWh.m^{-3}$ and 52.4 $kWh.m^{-3}$, for MCD and UNCD anodes, respectively.

ACKNOWLEDGEMENTS

Financial support from the projects CTM2013-44081-R, CTM2016-75509-R and to the Spanish Excellence Network E3TECH (CTQ2015-71650-RDT) (MINECO, SPAIN-FEDER 2014–2020) is gratefully acknowledged. B. Gomez also thanks the FPI research scholarship (BES-2014-071045). Dr. J. Carrillo-Abad is gratefully acknowledged for performing the cyclic voltammograms included in supplementary data.

REFERENCES

[1] E. Brillas, C.A. Martinez-Huitle, Synthetic Diamond Films, John Wiley & Sons, Inc., Hoboken, NJ, USA, 2011.

[2] R.G. Compton, J.S. Foord, F. Marken, Electroanalysis at diamond-like and doped-diamond electrodes, Electroanalysis. 15 (2003) 1349–1363. doi:10.1002/elan.200302830.

[3] M.A. Rodrigo, P. Cañizares, A. Sánchez-Carretero, C. Sáez, Use of conductive-diamond electrochemical oxidation for wastewater treatment, Catal. Today. 151 (2010) 173–177. doi:10.1016/j.cattod.2010.01.058.

[4] J.H.T. Luong, B. Male, J.D. Glennon, K.B. Male, J.D. Glennon, Boron-doped diamond electrode: synthesis, characterization, functionalization and analytical applications., Analyst. 134 (2009) 1965–79. doi:10.1039/b910206j.

[5] F.L. Souza, C. Saéz, M.R. V Lanza, P. Cañizares, M.A. Rodrigo, The effect of the sp3/sp2 carbon ratio on the electrochemical oxidation of 2,4-D with p-Si BDD anodes, Electrochim. Acta. 187 (2016) 119–124. doi:10.1016/j.electacta.2015.11.031.

[6] J.M. Peralta-Hernández, M. Méndez-Tovar, R. Guerra-Sánchez, C.A. Martínez-Huitle, J.L. Nava, A Brief Review on Environmental Application of Boron Doped Diamond Electrodes as a New Way for Electrochemical Incineration of Synthetic Dyes, Int. J. Electrochem. 2012 (2012) 1–18. doi:10.1155/2012/154316.

[7] A. Fernandes, D. Santos, M.J. Pacheco, L. Ciríaco, A. Lopes, Nitrogen and organic load removal from sanitary landfill leachates by anodic oxidation at Ti/Pt/PbO_2, Ti/Pt/SnO_2-Sb_2O_4 and Si/BDD, Appl. Catal. B Environ. 148–149 (2014) 288–294. doi:10.1016/j.apcatb.2013.10.060.

[8] A. Kraft, Doped Diamond: A Compact Review on a New, Versatile Electrode Material - Open Access Library, Int. J. Electrochem. Sci. 2 (2007) 355–385. doi:10.1021/jo026183k.

[9] T.A. Ivandini, Y. Einaga, Polycrystalline boron-doped diamond electrodes for electrocatalytic and electrosynthetic applications, Chem. Commun. 53 (2017) 1338–1347. doi:10.1039/C6CC08681K.

[10] I. Sirés, E. Brillas, M.A. Oturan, M.A. Rodrigo, M. Panizza, Electrochemical advanced oxidation processes: Today and tomorrow. A review, Environ. Sci. Pollut. Res. 21 (2014) 8336–8367. doi:10.1007/s11356-014-2783-1.

[11] C. Di Dong, T.S. Chen, C.W. Chen, K.L. Huang, Electrochemical degradation of diethyl phthalate under different operating conditions, Int. J. Electrochem. Sci. 11 (2016) 5009–5020. doi:10.20964/2016.06.77.

[12] A.M. Urtiaga, G. Pérez, R. Ibáñez, I. Ortiz, Removal of pharmaceuticals from a WWTP secondary effluent by ultrafiltration/reverse osmosis followed by electrochemical oxidation of the RO concentrate, Desalination. 331 (2013) 26–34. doi:10.1016/J.DESAL.2013.10.010.

[13] A.M. Trautmann, H. Schell, K.R. Schmidt, K.M. Mangold, A. Tiehm, Electrochemical degradation of perfluoroalkyl and polyfluoroalkyl substances (PFASs) in groundwater, Water Sci. Technol. 71 (2015) 1569–1575. doi:10.2166/wst.2015.143.

[14] B. Gomez-Ruiz, S. Gómez-Lavín, N. Diban, V. Boiteux, A. Colin, X. Dauchy, A. Urtiaga, Efficient electrochemical degradation of poly- and perfluoroalkyl substances (PFASs) from the effluents of an industrial wastewater treatment plant, Chem. Eng. J. 322 (2017). doi:10.1016/j.cej.2017.04.040.

[15] C.E. Schaefer, C. Andaya, A. Burant, C.W. Condee, A. Urtiaga, T.J. Strathmann, C.P. Higgins, Electrochemical treatment of perfluorooctanoic acid and perfluorooctane sulfonate: insights into mechanisms and application to groundwater treatment, Chem. Eng. J. (2017). doi:10.1016/j.cej.2017.02.107.

[16] S.H. Prevedouros, Konstantinos; Cousins, Ian T.; Buck, Robert C., Korzeniowski, Critical Review Sources , Fate and Transport of Fate, Environ. Sci. Technol. 40 (2006) 32–44. doi:10.1021/es0512475.

[17] X.C. Hu, D.Q. Andrews, A.B. Lindstrom, T.A. Bruton, L.A. Schaider, P.

Grandjean, R. Lohmann, C.C. Carignan, A. Blum, S.A. Balan, C.P. Higgins, E.M. Sunderland, Detection of Poly- and Perfluoroalkyl Substances (PFASs) in U.S. Drinking Water Linked to Industrial Sites, Military Fire Training Areas, and Wastewater Treatment Plants, Environ. Sci. Technol. Lett. 3 (2016) 344–350. doi:10.1021/acs.estlett.6b00260.

[18] K.E. Carter, J. Farrell, Oxidative destruction of perfluorooctane sulfonate using boron-doped diamond film electrodes, Environ. Sci. Technol. 42 (2008) 6111–6115. doi:10.1021/es703273s.

[19] H. Xiao, B. Lv, G. Zhao, Y. Wang, M. Li, D. Li, Hydrothermally enhanced electrochemical oxidation of high concentration refractory perfluorooctanoic acid, J. Phys. Chem. A. 115 (2011) 13836–13841. doi:10.1021/jp207519j.

[20] T. Ochiai, Y. Iizuka, K. Nakata, T. Murakami, D.A. Tryk, Y. Koide, Y. Morito, A. Fujishima, Efficient decomposition of perfluorocarboxylic acids in aqueous suspensions of a TiO_2 photocatalyst with medium-pressure ultraviolet lamp irradiation under atmospheric pressure, Ind. Eng. Chem. Res. 50 (2011) 10943–10947. doi:10.1021/ie1017496.

[21] H. Lin, J. Niu, J. Xu, H. Huang, D. Li, Z. Yue, C. Feng, Highly efficient and mild electrochemical mineralization of long-chain perfluorocarboxylic acids (C9-C10) by Ti/SnO_2-Sb-Ce, Ti/SnO_2-Sb/Ce-PbO_2, and Ti/BDD electrodes, Environ. Sci. Technol. 47 (2013) 13039–13046. doi:10.1021/es4034414.

[22] Á. Soriano, D. Gorri, A. Urtiaga, Efficient treatment of perfluorohexanoic acid by nanofiltration followed by electrochemical degradation of the NF concentrate, Water Res. 112 (2017) 147–156. doi:10.1016/j.watres.2017.01.043.

[23] Q. Zhuo, S. Deng, B. Yang, J. Huang, B. Wang, T. Zhang, G. Yu, Degradation of perfluorinated compounds on a boron-doped diamond electrode, Electrochim. Acta. 77 (2012) 17–22. doi:10.1016/j.electacta.2012.04.145.

[24] Z. Liao, J. Farrell, Electrochemical oxidation of perfluorobutane sulfonate using boron-doped diamond film electrodes, J. Appl. Electrochem. 39 (2009) 1993–1999. doi:10.1007/s10800-009-9909-z.

[25] D. Medeiros De Araújo, P. Cañizares, C.A. Martínez-Huitle, M.A. Rodrigo, Electrochemical conversion/combustion of a model organic pollutant on BDD anode: Role of sp^3/sp^2 ratio, Electrochem. Commun. 47 (2014) 37–40. doi:10.1016/j.elecom.2014.07.017.

[26] E. Guinea, F. Centellas, E. Brillas, P. Cañizares, C. Sáez, M.A. Rodrigo, Electrocatalytic properties of diamond in the oxidation of a persistant pollutant, Appl. Catal. B Environ. 89 (2009) 645–650. doi:10.1016/j.apcatb.2009.01.028.

[27] S. Fierro, K. Abe, C. Comninellis, Y. Einaga, Influence of doping level on the electrochemical oxidation of formic acid on boron doped diamond electrodes, J. Electrochem. Soc. 158 (2011). doi:10.1149/2.050112jes.

[28] S. Garcia-Segura, E. Vieira dos Santos, C.A. Martínez-Huitle, Role of sp^3/sp^2 ratio on the electrocatalytic properties of boron-doped diamond electrodes: A mini review, Electrochem. Commun. 59 (2015) 52–55. doi:10.1016/J.ELECOM.2015.07.002.

[29] J. Zhang, J.W. Zimmer, R.T. Howe, R. Maboudian, Characterization of boron-doped micro- and nanocrystalline diamond films deposited by wafer-scale hot filament chemical vapor deposition for MEMS applications, Diam. Relat. Mater. 17 (2008) 23–28. doi:10.1016/j.diamond.2007.09.010.

[30] E. Yasu, N. Ohashi, T. Ando, J. Tanaka, M. Kamo, Y. Sato, H. Kiyota, Hall mobility and carrier concentration of boron-doped homoepitaxially grown diamond (001) films, Diam. Relat. Mater. 4 (1994) 59–61. doi:10.1016/0925-9635(94)90069-8.

[31] H. Nagasaka, Y. Teranishi, Y. Kondo, T. Miyamoto, T. Shimizu, Growth Rate and Electrochemical Properties of Boron-Doped Diamond Films Prepared by Hot-Filament Chemical Vapor Deposition Methods, E-Journal Surf. Sci. Nanotechnol. 14 (2016) 53–58. doi:10.1380/ejssnt.2016.53.

[32] M.R. Baldan, A.F. Azevedo, A.B. Couto, N.G. Ferreira, Cathodic and anodic pre-treated boron doped diamond with different sp^2 content: Morphological, structural, and impedance spectroscopy characterizations, J. Phys. Chem. Solids. 74 (2013) 1830–1835. doi:10.1016/j.jpcs.2013.07.015.

[33] J. V Macpherson, A practical guide to using boron doped diamond in electrochemical research., Phys. Chem. Chem. Phys. 17 (2015) 2935–49. doi:10.1039/c4cp04022h.

[34] S. Ohmagari, T. Yoshitake, A. Nagano, R. Ohtani, H. Setoyama, E. Kobayashi, T. Hara, K. Nagayama, Formation of p-type semiconducting ultrananocrystalline diamond/hydrogenated amorphous carbon composite films by boron doping, Jpn. J. Appl. Phys. 49 (2010). doi:10.1143/JJAP.49.031302.

[35] H. Zeng, A.R. Konicek, N. Moldovan, F. Mangolini, T. Jacobs, I. Wylie, P.U. Arumugam, S. Siddiqui, R.W. Carpick, J.A. Carlisle, Boron-doped ultrananocrystalline diamond synthesized with an H-rich/Ar-lean gas system, Carbon N. Y. 84 (2015) 103–117. doi:10.1016/j.carbon.2014.11.057.

[36] B.P. Chaplin, I. Wyle, H. Zeng, J.A. Carlisle, J. Farrell, Characterization of the performance and failure mechanisms of boron-doped ultrananocrystalline diamond electrodes, J. Appl. Electrochem. 41 (2011) 1329–1340. doi:10.1007/s10800-011-0351-7.

[37] A. Urtiaga, C. Fernández-González, S. Gómez-Lavín, I. Ortiz, Kinetics of the electrochemical mineralization of perfluorooctanoic acid on ultrananocrystalline boron doped conductive diamond electrodes, Chemosphere. 129 (2015) 20–26. doi:10.1016/j.chemosphere.2014.05.090.

[38] APHA (American Public Health Association), Standard Methods for the Examination of Water and Wastewater, 20th Ed., Washington DC, 1998. doi:ISBN 9780875532356.

[39] A. Urtiaga, A. Soriano, J. Carrillo-Abad, BDD anodic treatment of 6:2 fluorotelomer sulfonate (6:2 FTSA). Evaluation of operating variables and by-product formation, Chemosphere. (2018). doi:10.1016/j.chemosphere.2018.03.027.

[40] M. Mascia, A. Vacca, S. Palmas, A.M. Polcaro, Kinetics of the electrochemical oxidation of organic compounds at BDD anodes: Modelling of surface reactions, J. Appl. Electrochem. 37 (2007) 71–76. doi:10.1007/s10800-006-9217-9.

[41] M. Panizza, G. Siné, I. Duo, L. Ouattara, C. Comninellis, Electrochemical Polishing of Boron-Doped Diamond in Organic Media, Electrochem. Solid-State Lett. 6 (2003) D17–D19. doi:10.1149/1.1619646.

[42] B. Guan, J. Zhi, X. Zhang, T. Murakami, A. Fujishima, Electrochemical route for fluorinated modification of boron-doped diamond surface with perfluorooctanoic acid, Electrochem. Commun. 9 (2007) 2817–2821. doi:10.1016/j.elecom.2007.10.003.

[43] B. Yang, C. Jiang, G. Yu, Q. Zhuo, S. Deng, J. Wu, H. Zhang, Highly efficient electrochemical degradation of perfluorooctanoic acid (PFOA) by F-doped Ti/SnO2 electrode, J. Hazard. Mater. 299 (2015) 417–424. doi:10.1016/j.jhazmat.2015.06.033.

[44] P. Cañizares, C. Sáez, A. Sánchez-Carretero, M.A. Rodrigo, Influence of the characteristics of p-Si BDD anodes on the efficiency of peroxodiphosphate electrosynthesis process, Electrochem. Commun. 10 (2008) 602–606. doi:10.1016/j.elecom.2008.01.038.

[45] Advanced Diamond Technologies, (2016). http://www.thindiamond.com/uncd-technology/what-is-uncd/ (accessed November 20, 2017).

[46] P.W. May, W.J. Ludlow, M. Hannaway, P.J. Heard, J.A. Smith, K.N. Rosser, Raman and conductivity studies of boron-doped microcrystalline diamond, facetted nanocrystalline diamond and cauliflower diamond films, Diam. Relat. Mater. 17 (2008) 105–117. doi:10.1016/j.diamond.2007.11.005.

[47] P. Szirmai, T. Pichler, O.A. Williams, S. Mandal, C. Bäuerle, F. Simon, A detailed analysis of the Raman spectra in superconducting boron doped nanocrystalline diamond, Phys. Status Solidi. 249 (2012) 2656–2659. doi:10.1002/pssb.201200461.

[48] W. Gajewski, P. Achatz, O.A. Williams, K. Haenen, E. Bustarret, M. Stutzmann, J.A. Garrido, Electronic and optical properties of boron-doped nanocrystalline diamond films, Phys. Rev. B - Condens. Matter Mater. Phys. 79 (2009) 1–14. doi:10.1103/PhysRevB.79.045206.

[49] H. Kuzmany, R. Pfeiffer, N. Salk, B. Günther, The mystery of the 1140 cm^{-1} Raman line in nanocrystalline diamond films, Carbon N. Y. 42 (2004) 911–917. doi:10.1016/j.carbon.2003.12.045.

[50] V. Mortet, L. Zhang, M. Eckert, J. D'Haen, A. Soltani, M. Moreau, D. Troadec, E. Neyts, J.C. De Jaeger, J. Verbeeck, A. Bogaerts, G. Van Tendeloo, K. Haenen, P. Wagner, Grain size tuning of nanocrystalline chemical vapor deposited diamond by continuous electrical bias growth: Experimental and theoretical study, Phys. Status Solidi Appl. Mater. Sci. 209 (2012) 1675–1682. doi:10.1002/pssa.201200581.

[51] M. Wang, N. Simon, G. Charrier, M. Bouttemy, A. Etcheberry, M. Li, R. Boukherroub, S. Szunerits, Distinction between surface hydroxyl and ether groups on boron-doped diamond electrodes using a chemical approach, Electrochem. Commun. 12 (2010) 351–354. doi:10.1016/j.elecom.2009.12.029.

[52] D. Ballutaud, N. Simon, H. Girard, E. Rzepka, B. Bouchet-Fabre, Photoelectron spectroscopy of hydrogen at the polycrystalline diamond surface, Diam. Relat. Mater. 15 (2006) 716–719. doi:10.1016/j.diamond.2006.01.004.

[53] R. Bogdanowicz, A. Fabiańska, L. Golunski, M. Sobaszek, M. Gnyba, J. Ryl, K. Darowicki, T. Ossowski, S.D. Janssens, K. Haenen, E.M. Siedlecka, Influence of the boron doping level on the electrochemical oxidation of the azo dyes at Si/BDD thin film electrodes, Diam. Relat. Mater. 39 (2013) 122–127. doi:10.1016/j.diamond.2013.08.004.

[54] S.C. Ramos, A.F. Azevedo, M.R. Baldan, N.G. Ferreira, Effect of methane addition on ultrananocrystalline diamond formation: Morphology changes and induced stress, J. Vac. Sci. & Technol. A-Vacuum Surfaces Film. 28 (2010) 27–32. doi:10.1116/1.3259885.

[55] Y. Feng, J. Lv, J. Liu, N. Gao, H. Peng, Y. Chen, Influence of boron concentration on growth characteristic and electro-catalytic performance of boron-doped diamond electrodes prepared by direct current plasma chemical vapor deposition, Appl. Surf. Sci. 257 (2011) 3433–3439. doi:10.1016/j.apsusc.2010.11.041.

[56] O. Andrade, L. S., Salazar-Banda, G. R., Rocha-Filho, R. C. and Fatibello-Filho, 8. Cathodic Pretreatment of Boron-Doped Diamond Electrodes and their Use in Electroanalysis, in: E. Brillas, C.A. Martínez-Huitle (Eds.), Synth. Diam. Film. Prep. Electrochem. Charact. Appl., John Wiley & Sons, Inc., Hoboken, NJ, USA, 2011.

[57] G.R. Salazar-Banda, L.S. Andrade, P.A.P. Nascente, P.S. Pizani, R.C. Rocha-Filho, L.A. Avaca, On the changing electrochemical behaviour of boron-doped diamond surfaces with time after cathodic pre-treatments, Electrochim. Acta. 51 (2006) 4612–4619. doi:10.1016/j.electacta.2005.12.039.

[58] Á. Anglada, A. Urtiaga, I. Ortiz, Contributions of electrochemical oxidation to waste-water treatment: Fundamentals and review of applications, J. Chem. Technol. Biotechnol. 84 (2009) 1747–1755. doi:10.1002/jctb.2214.

SUPPORTING INFORMATION

Comparison of microcrystalline and ultrananocrystalline boron doped diamond anodes: Influence on perfluorooctanoic acid electrolysis

Authors:

Beatriz Gomez-Ruiz, Nazely Diban*, Ane Urtiaga

Department of Chemical and Biomolecular Engineering. University of Cantabria. Av. de Los Castros s/n. 39005 Santander. Spain

* Corresponding Author: dibann@unican.es

Submitted to

Separation and Purification Technology

March 2018

Table S1. Summary of the BDD-electrochemical oxidation for PFASs degradation in aqueous media.

Reference	EXPERIMENTAL CONDITIONS				ELECTROCHEMICAL PERFORMANCE	
	Characteristics of BDD	**Configuration**	***J* (mA.cm^{-2})**	**Feed Volume (L)**	**[PFAS]$_{initial}$ (mM)**	***k'* (h^{-1})**
Carter and Farrell., 2008 [18]	One bipolar and two monopolar p-Si/BDD electrodes (Adamant Technologies). Total anode area: 25 cm^2	Parallel plate flow-through reactor	20	2	0.4 mM PFOS	7.8
Liao and Farrell., 2009 [24]	One bipolar and two monopolar p-Si/BDD electrodes (Adamant Technologies). Total anode area: 25 cm^2	Flow-through reactor	10	0.35 or 0.6	0.4 mM PFBS	(>90 % degradation, 1h)
Ochiai et al., 2011 [20]	BDD electrode (Condias). Anode area: 77.4 cm^2	Single compartment flow cell	0.15	0.3	8 mM PFOA	0.8
Xiao et al., 2011 [19]	Si/BDD electrode, boron doping of 1300 ppm and thickness of the diamond film is about 1 μm (CVD). Anode area: 5.5 cm^2	Teflon-lined stainless steel autoclave cell	20	0.4	0.48 mM PFOA	0.108
Zhuo et al., 2012 [23]	Si/BDD (Chinese Academy of Science). Anode area: 8.5 cm^2	Three-electrode cell	23.24	0.04	0.114 mM PFBA 0.114 mM PFHxA 0.114 mM PFOA 0.114 mM PFDeA	1.992 2.01 2.568 2.73

					0.114 mM PFBS 0.114 mM PFHxS 0.114 mM PFOS	0.834 1.338 2.142
Lin et al., 2013 [21]	Ti/BDD electrode (HF CVD) (Condias). Anode area: 25 cm^2	Undivided electrochemical cell	10	0.1	0.25 mM PFNA 0.25 mM PFDA	1.38 1.08
Trautmann et al., 2015 [13]	Nb/BDD electrode (Condias). Anode area: 35 cm^2	Undivided electrochemical cell	2.3	1	0.0097 mM PFBS 0.0275 mM PFHxS 0.030 mM PFOS	(43%, 91% and 98% degradation after 43h, respectively)
Schaefer et al., 2017 [15]	Nb/Ultrananocrystalline diamond coating (Advanced Diamond Technologies). Anode area: 38 cm^2	Single compartment flow-by cell	3, 15 and 50 50 15 15	0.25	0.036 mM PFOA 0.020 mM PFOS 0.0007 mM PFOA 0.0012 mM PFOS	0.091, 0.37 and 1.4 0.37 0.33 0.12
Soriano et al., 2017 [22]	One bipolar and two monopolar p-Si/BDD electrodes (Adamant Technologies). Anode area: 140 cm^2	Undivided cell with two parallel flow-by compartments	50	1	2.17 mM PFHxA	1.764

Abbreviations: *j*: applied current density; *k*: degradation kinetic constant; HF CVD: Hot-filament chemical vapor deposition; CVD: Chemical vapor deposition

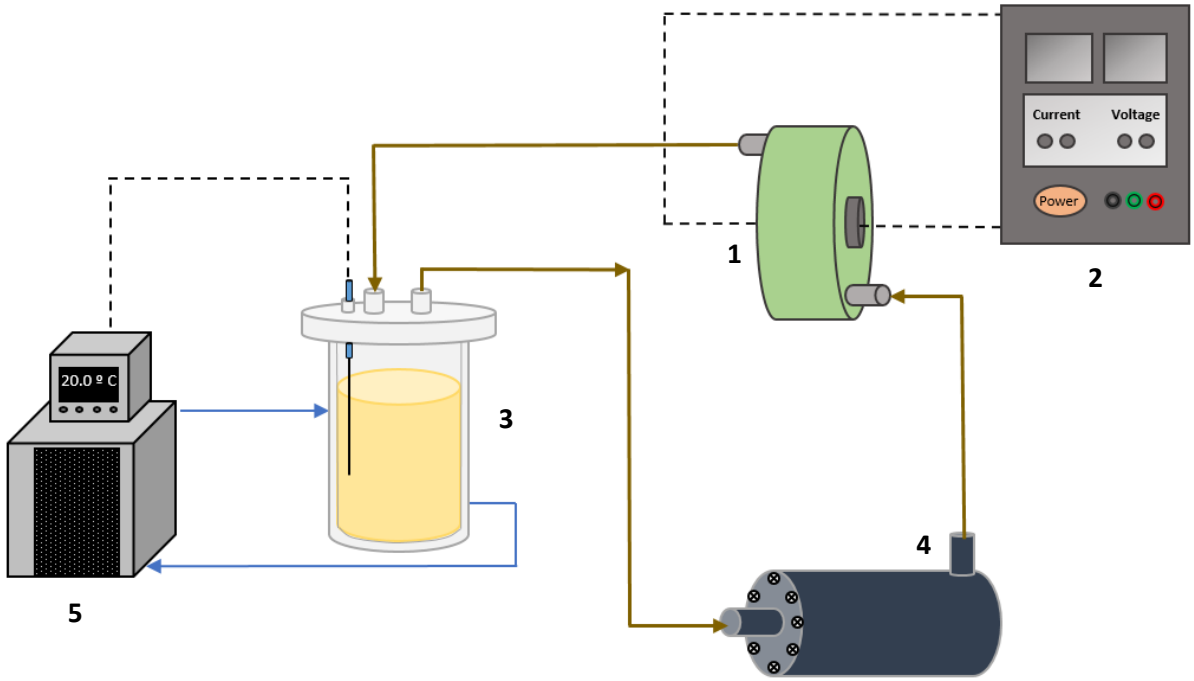

Figure S1. Electro-oxidation experimental system (1: Single Compartment Electrochemical Cell, 2: Power Supply, 3: Feed Tank, 4: Pump, 5: Refrigeration System).

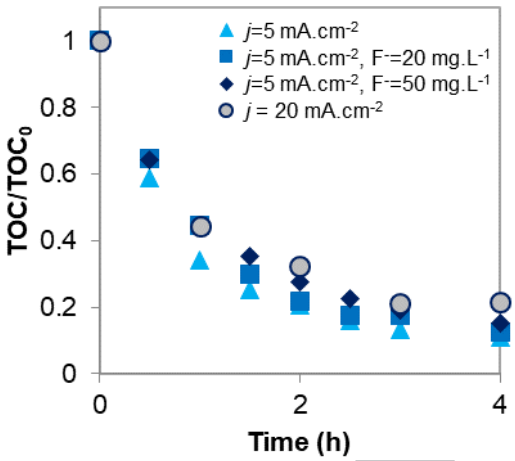

Figure S2. Influence of fluoride added in the reacting media on TOC removal with the electro-oxidation time using MCD anode at j = 5 mA.cm^{-2} with no addition of F$^-$ (▲), at j = 5 mA.cm^{-2} adding 20 mg.L^{-1} of F$^-$ (■), at j = 5 mA.cm^{-2} adding 50 mg.L^{-1} of F$^-$ (◆) and at j = 20 mA.cm^{-2} with no addition of F$^-$ (○). $[PFOA]_0$ = 0.24 mmol.L^{-1}

Cyclic voltammetries were performed in a three-electrode cell using 50 mL PFOA (0.24 mmol.L^{-1}) and 5 g.L^{-1} Na_2SO_4 as electrolyte. Ag/AgCl saturated KCl electrode was used as the reference electrode and the counter electrode was a Pt foil. MCD and UNCD were used as working electrodes. For these tests, 1x1 cm^2 samples of the commercial electrodes were obtained by fracture of the original ones.

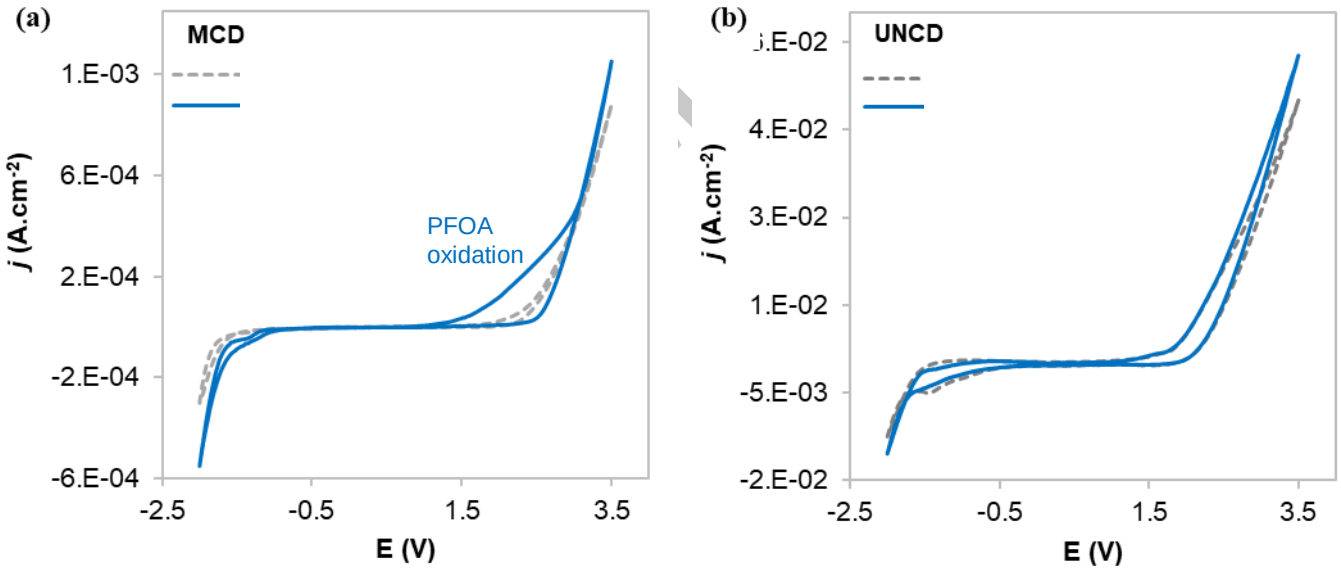

Figure S3. Cyclic voltammogram of 0.24 mmol.L^{-1} of PFOA (blue lines) in 5 g.L^{-1} Na_2SO_4 solutions for (a) MCD and (b) UNCD anodes, obtained at 100 mV.s^{-1} of scan rate. Cyclic voltammograms of single Na_2SO_4 (dotted lines) are included for comparison.

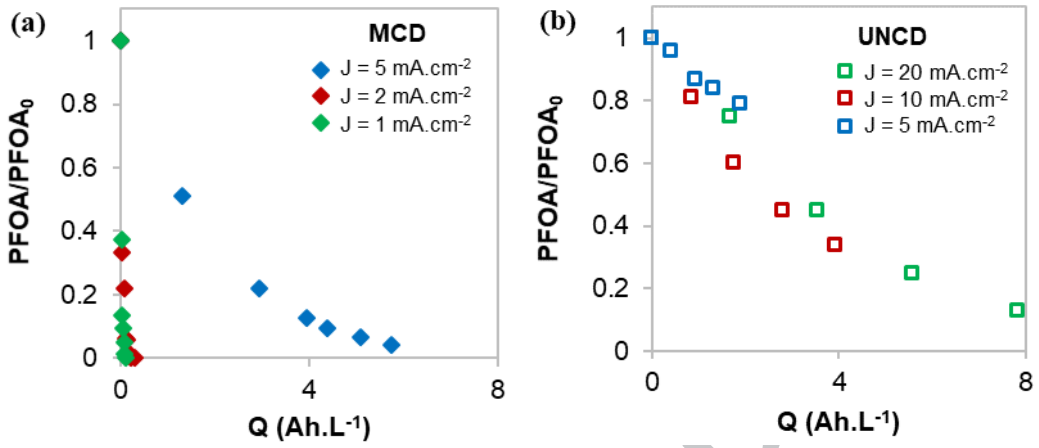

Figure S4. PFOA dimensionless evolution as a function of specific electrical charge (Q) using: (a) MCD anode (j = 1, 2 and 5 mA.cm^{-2}) and (b) UNCD anode (j = 5, 10 and 20 mA.cm^{-2}). $[PFOA]_0$ = 0.24 mmol.L^{-1}

Highlights

- Microcrystalline (MCD) and ultrananocrystalline (UNCD) BDD anodes were compared
- MCD exhibited 50-fold higher PFOA removal rate than UNCD
- PFOA (0.24 mmol.L^{-1}) removal using MCD was achieved at only 1.4 kWh.m^{-3}
- MCD contained more carbon sp^3, less H-terminated carbon and less boron than UNCD
- Electrochemical function relates to crystal & chemical properties of diamond films

Graphical Abstract